Pharmaceutical Research (2025) 42:1385–1396
https://doi.org/10.1007/s11095-025-03888-2

ORIGINAL RESEARCH ARTICLE

# Investigating Zinc Migration from Rigid Needle Shield to Drug Formulation in Needle Tip of Pre-filled Syringe

**Guangli Hu[1] · Chengbei Li[2] · Kaitlin Wang[1] · Yongchao Su[1] · William Forrest[1] · Jeffrey Givand[1] · Dario Ferreira Sanchez[4] · Margie Olbinado[3,4] · Matthias Wagner[3] · Christian Grünzweig[3] · Vladimir Novak[3]**

Received: 14 March 2025 / Accepted: 21 June 2025 / Published online: 29 July 2025


## Abstract

**Objective** This study investigates the underexplored mechanisms of needle clogging in pre-filled syringes (PFSs), focusing on zinc (Zn) ions, which have been reported to promote protein gelation and increase formulation viscosity. We present direct evidence of Zn migration from the rigid needle shield (RNS) into drug products, aiming to elucidate the migration pathways and the role of Zn in clogging.

**Methods** Pre-filled syringes containing a therapeutic monoclonal antibody (mAb) were stored at 5°C and subjected to stress conditions at 40°C for up to six months. Inductively coupled plasma mass spectrometry (ICP-MS) measured metal ion levels, while synchrotron-based X-ray phase-contrast computed tomography (SR-XPCT) and X-ray fluorescence (SR-XRF) provided *in situ* visualization of Zn distribution in dry materials under stress.

**Results** We found that Zn leaches from the RNS into the drug formulation during liquid-RNS contact. ICP-MS revealed higher Zn levels, along with aluminum and titanium, in clogged needles compared to clean ones. SR-XRF identified Zn hot spots within the dried drug product, while SR-XPCT displayed 3D visualization of Zn particle accumulation at the needle tip. Notably, Zn migration accelerated at 40°C, with minimal detection at 5°C, indicating the significant influence of temperature.

**Conclusions** This study offers the first experimental evidence of Zn migration from the RNS into drug formulations within staked-in-needle PFSs. While Zn is not solely responsible for needle clogging, its presence in both RNS and the drug suggests a contributory role. These insights can inform strategies for improving PFS performance and reliability.

**Keywords** Clogging · High concentration biologics · Pre-filled syringes · Rigid needle shield · Zinc

## Introduction

Staked-in-needle pre-filled syringes (PFSs) are becoming widely utilized in drug-device combination products to enable patient-centered drug delivery. These syringes allow for administration outside of clinical settings by patients or lay users, improving accessibility and reducing costs [1]. One issue that emerged with the use of staked-in-needle PFSs is needle clogging, particularly in higher concentration and subcutaneous protein drug products [2, 3]. These high concentration formulations at ≥ 100 mg/mL protein concentration often have increased viscosity [3] which can impede fluid flow and increase the likelihood of needle clogging [4]. The risk of needle clogging in high concentration formulations has been recognized in regulatory filings, and there have been incidents of needle clogging leading to product recalls [2, 5–7]. For example, needle clogging in low concentration formulations like SYMJEPI® (Epinephrine) (0.5–1.0 mg/mL) resulted in a voluntary product recall, highlighting the need to understand the underlying mechanisms beyond water evaporation through the rigid needle shield (RNS) [5].

✉ Guangli Hu
guangli.hu@merck.com

✉ Yongchao Su
yongchao.su@merck.com

1 Pharmaceutical Sciences and Clinical Supply, Merck & Co., Inc, Rahway, NJ 07065, USA

2 Analytical Research & Development, Merck & Co., Inc, Rahway, NJ 07065, USA

3 ANAXAM, Park Innovaare, Parkstrasse 1, CH-5234 Villigen, Switzerland

4 Paul Scherrer Institute, Forschungsstrasse 111, 5232 Villigen PSI, Switzerland

The root cause of needle clogging in staked-in-needle PFSs is multifaceted, involving complex interactions between formulation components, device materials, and storage conditions [8–11]. One proposed mechanism suggests that liquid entering the needle experiences water vapor loss through the RNS, leading to drying and clogging. Using neutron imaging, water vapor transmission rate was shown to be dependent on RNS formulation, with migration of the drug product into the needle being dependent on storage conditions, leading to clogging [12]. A recent scientific report suggests chemical stability factors also potentially contribute, such as Zn migration from the rigid needle shield, in increasing the viscosity, causing gelation, and exacerbating clogging under certain conditions [13]. However, direct confirmation of any metal ions, particularly Zn, migrating into the drug product has not been provided until now. Fukuda *et al.* demonstrated that the use of dynamic light scattering, and small-angle X-ray scattering can provide valuable information about the reactivity of mAb systems with Zn ions and that this reactivity accelerates needle clogging. The study underscored the impact of diverse factors, including buffer conditions, mAb chemistry, and the nature of the RNS elastomer, on the colloidal stability of mAb solutions [13]. Previous works have leveraged neutron imaging to view drug product accumulation in the needle, with a resolution of ~ 50 µm depending on the system, however these sources do not provide chemical information [14].

The advancement and utilization of cutting-edge imaging techniques provide new opportunities to investigate device-related behaviors, offering valuable insights into the mechanisms underlying needle clogging in pre-filled syringes. For example, while routine X-ray computed tomography is not suitable for visualizing low-density liquids in stainless-steel needles, the development of phase-contrast computed tomography using partially coherent X-ray beams available at synchrotron sources has made it possible to visualize liquid in small cavities and formulation movement under temperature and pressure cycling [10, 15]. Importantly, such cycling was found to cause localized formulation accumulations at the needle tip, increasing the risk of needle clogging. Synchrotron-based X-ray phase-contrast computed tomography (SR-XPCT) has also been leveraged to gather insights into the injectability of drug product into tissue [16, 17]. In order to qualitatively analyze elements of the dried drug in the needle tip, synchrotron-based X-ray fluorescence (SR-XRF) spectroscopy can be used [10]. With a scanning micro-focused X-ray beam SR-XRF analysis enables visualizing the spatial distribution of elemental composition with micrometer resolution.

Moreover, quantification and visualization of ion content is important to elucidate the key factors (such as time and temperature) that induce leaching [13]. Suitable for inorganic elements, inductively coupled plasma mass spectrometry (ICP-MS) has been previously applied to study silicone oil migration and trace element analysis [13, 21–23]. ICP-MS provides quantification of silicone oil migration content in syringe systems and can identify Zn content [20, 21].

Despite the hypothetical mechanism that Zn induces clogging, the existence of Zn migration from the rigid needle shield into protein formulation, has not yet been observed. In this study, SR-XRF, ICP-MS, and SR-XPCT are employed to explore migration of Zn into drug formulation in a qualitative and quantitative manner. The study aims to gain new insights into the phenomenon of needle clogging in pre-filled syringes and improve our understanding of RNS leaching. The application of these techniques provides valuable information for the development of strategies to mitigate needle clogging issues and improve the performance of pre-filled syringe systems.

## Materials and Methods

### Materials and Samples

The staked-in-needle PFS samples utilized in this study were composed of a siliconized Type I borosilicate clear glass barrel with a small round flange. The outer diameter of the barrel was measured at 8.65 ± 0.1 mm. The needle cannula, made of stainless steel, featured a 5-bevel design with an inner diameter corresponding to 27G thin wall needles (nominal ID of 270 µm) and a length of 12.7 mm. The RNS was constructed using a polyisoprene-based rubber formulation. The elastomer material of the needle shield demonstrated a moisture vapor transmission rate of 4.98 g/m$^2$ per day, as determined by ASTM F1249 testing conditions.

The syringes in this study were filled with a solution of monoclonal antibody (mAb) at a concentration of 165 mg/mL, which included surfactants and stabilizers. The filling and stoppering process was conducted using a lab-scale semi-automatic Groninger filling machine. FluroTec®-coated plunger stoppers were used to seal the syringes through the vent tube method.

Then, the syringes were staged at different environmental chambers for an aging study. Specifically, real time aging is at 5°C and accelerated aging is at 40°C/75% RH. Samples were tested on an Instron mechanical tester for break loose and extrusion force at specific time points. If the maximum force during testing is above 100 N, then the samples were considered fully clogged. Approximately 1500 samples were tested at 5°C. Out of these, only 1 sample was found to be clogged at the 6-month time point, which was analyzed in this study. Additional samples were staged at 40°C/75% RH and were tested at 1-, 2-, 3-, and 4-month time points. Once the sample is identified as clogged, then the samples were kept at 5°C until further analysis was conducted.

Table I summarizes conditions and the number of investigated samples with a corresponding analytical method. The syringes investigated with SR-XRF and SR-XPCT were the same, while those investigated with ICP-MS were different syringes but were from the same batch of conditioning.

## Mass Spectrometry

Mass spectrometry was used to identify and quantify the chemical composition of the samples by measuring the mass-to-charge ratio of ions. In this study, an Agilent 8900 triple quadrupole ICP-MS system (Agilent Technologies, USA) was used to effectively eliminate interference and obtain precise and accurate results. Several experiments were designed to provide a deeper understanding of the mechanism of clogging.

Due to the limited accessibility to the inside of the needle, the direct analysis of the metal content within the clogged material poses certain analytical challenges. The 69-metal scan method was developed in-house. We used three calibration standards to establish the calibration curve without internal standards, as they were included in the scan. To fulfill the purpose, we used a microwave digestion system. The samples (clean needle and clogged needle) were transferred into PTFE digestion tubes, and 1 ml of concentrated nitric acid was added. Samples were digested in the Milestone UltraWAVE system following the specified microwave program:

Step 1: 800 W, $T_1$ 110°C, $T_2$ 60°C, $P_1$ 90.0 bar, for 10 min
Step 2: 1200 W, $T_1$ 180°C, $T_2$ 60°C, $P_1$ 90.0 bar, for 10 min
Step 3: 1500 W, $T_1$ 250°C, $T_2$ 60°C, $P_1$ 110.0 bar, for 10 min

Step 4: 1500 W, $T_1$ 250°C, $T_2$ 60°C, $P_1$ 110.0 bar, for 10 min

For the clogged needles investigation, five syringes were chosen from a batch conditioned for 3 months at 40°C/75% RH. To quantify the mass of the clog, we first broke off needles from three fresh syringes and weighed them to establish a baseline. Subsequently, we broke off and weighed needles from clogged syringes, then calculated the average mass of the clogs. The average mass of the clog was determined to be 0.24 mg. To further investigate the metal sources, various combinations of samples, including water or drug product in combination with needles or RNS, were prepared and subjected to a 10-day stress test at a controlled temperature of 50°C. The solutions were tested by ICP-MS.

**Table I** Conditions of Syringes Analyzed. The Syringes were Stored Under Standard (5°C) and Stressed (40°C) Conditions for Varied Time Length

| Sample Conditions | ICP-MS | SR-XRF | SR-XPCT |
|---|---|---|---|
| 5°C for 6 months | N/A | 1 | 1 |
| 40°C for 2 months | N/A | 2 | 2 |
| 40°C for 3 months | 5 | 3 | 3 |
| 40°C for 4 months | N/A | 2 | 2 |

## Optical Microscopy

Images of clogs in the needle tip were acquired by Leica MZ16 optical microscope equipped with HIKVISION camera (model DS-2CD5085G0-AP).

## Synchrotron-based X-ray Phase-contrast Computed Tomography (SR-XPCT)

The conditioned syringes were examined using SR-XPCT at the TOMCAT beamline of the Swiss Light Source at the Paul Scherrer Institute, Switzerland. To mimic the storage orientation, the syringes were fixed in a needle-down position using a 3D-printed holder. A monochromatic beam with an X-ray energy of 30 keV was utilized. An X-ray image detector with a 150-µm LuAG:Ce scintillator lens-coupled with a 4× magnification microscope (Optique Peter, France) to a pco.edge 5.5 sCMOS camera (Excelitas Technologies, USA) was used. The effective pixel size was 1.6 µm, and the field-of-view was approximately $4.2 \times 3.0$ mm$^2$. To obtain the necessary data for tomography, a total of 1500 projections over a 180° rotation were acquired with an exposure time of 70 ms per frame. On some occasions, a monochromatic beam with an X-ray energy of 35 keV was used in combination with an X-ray image detector having an in-house built camera (GigaFRoST, PSI, Switzerland). The effective pixel size, in those cases, was 2.75 µm, and the field of view was $5.5 \times 3.0$ mm$^2$. A total of 3000 projections over a 180° rotation were acquired with an exposure time of 30 ms per frame. Eight tomographic scans were collected for each sample to cover the entire length of the needle, ranging from the needle tip to the glass barrel. To indicate which setup was used for a given image in the manuscript, the pixel size and X-ray energy are included in the figure captions.

## Synchrotron-based X-ray Fluorescence (SR-XRF) Spectroscopy

Elemental distribution mapping of the rigid needle shield and clogged needles was conducted at the micro-XAS beamline (X05LA) at the Swiss Light Source (Paul Scherrer Institute, SLS, Switzerland). First, measurements using an 18.1 keV incident beam were carried out with 40 s integration time, in order to examine the composition

of the rubber used in the RNS. In order to identify distribution of metallic elements in the dried drug of a needle, the incident beam was focused down to about 2 µm by 2 µm (H × V) using a Kirkpatrick-Baez (KB) mirror and selecting 12 keV as the incoming energy, to increase the sensitivity to Zn. The samples were raster-scanned in fly mode, with a step size of 4 µm and 100 ms integration time per pixel. Four XRF single-element silicon drift detectors (Ketek GmbH, Germany) coupled to FalconX pulse processors (XIA LLC, USA) were placed at about 30 mm from the sample position at respective angles of about 50° (front-left), 50° (front-right), 50° (back-left) and 50° (back-right) with respect to the beam path, Fig. 1 (right). The shape of the needles allowed the use of only the two back positioned ones, due to shadowing produced by the metallic needle.

## Results

Needle clogging in staked-in-needle PFSs presents significant challenges to drug delivery and product reliability. We aim to investigate metal migration, particularly Zn, due to its potential contribution to needle clogging, specifically focusing on identifying their origins from device components and how they migrate into the liquid formulation. We first use ICP-MS to examine the types and levels of metals in the clogged and cleaned needles, and then collect a comprehensive set of imaging data using SR-XPCT and SR-XRF to analyze metal content and distribution in clogged needles.

### Identification and Quantification of Metal Ions using ICP-MS and SR-XRF

We started with ICP-MS analysis of the clogged materials and aimed to examine, for the first time, the presence of Zn ions in the clogged material from syringes in real-life shelf-life study. Clogging was observed in PFS sealed with RNS and stored at elevated temperatures, as summarized in Table I. By subjecting the needles and clogged materials to high temperatures and pressures, the metals present therein were effectively released into a solution with the aid of concentrated nitric acid. Furthermore, to eliminate any potential metal background originating from the needles, a clean needle was also subjected to the digestion process and utilized as a reference. The clogged needle was dissolved in 1 mL of nitric acid and then diluted 10 times.

In our study, a full metal scan containing 69 elements was performed on the digested solutions of both clean and clogged needles conditioned for 3 months at 40°C/75% RH, Fig. 2. Zn, aluminum (Al), and titanium (Ti) present the largest differences between the clean and clogged needle. Considering the identical drug products filled in syringes with clean and clogged needles, the elevated levels of metals, such as Zn, must come from the syringe components. One source of Zn, as previously suggested was the RNS [13] Zn concentration (raw data) on the instrument was 350 ng. Considering the mass of the clog is 0.24 mg, the estimated Zn concentration in clogged material is 1.5 µg/mg.

To confirm the origin of Zn, Al, and Ti and explore the potential interaction between drug product (DP) and RNS, a series of four sample sets were prepared. In this study,

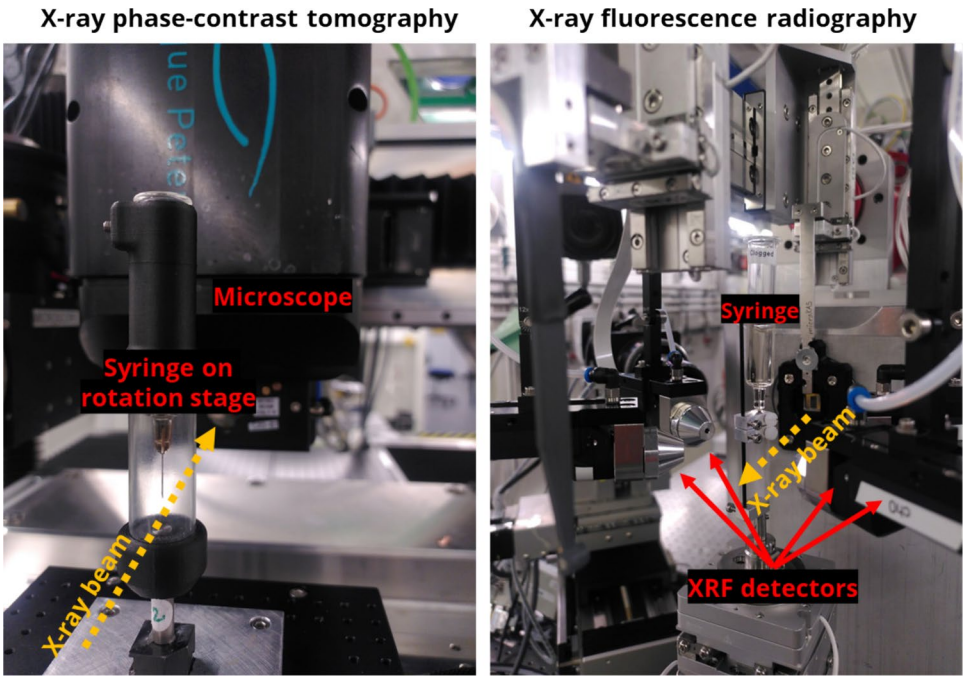


**Fig. 1** Imaging analysis using synchrotron-based X-ray phase-contrast computed tomography (SR-XPCT, left) and synchrotron-based X-ray fluorescence (SR-XRF, right). A syringe is mounted on the rotation stage at the TOMCAT beamline, Swiss Light Source (SLS), to acquire 3D images of the needle by SR-XPCT. The 2D images with chemical information were obtained by SR-XRF at microXAS beamline, SLS, by placing four detectors around the needle tip.

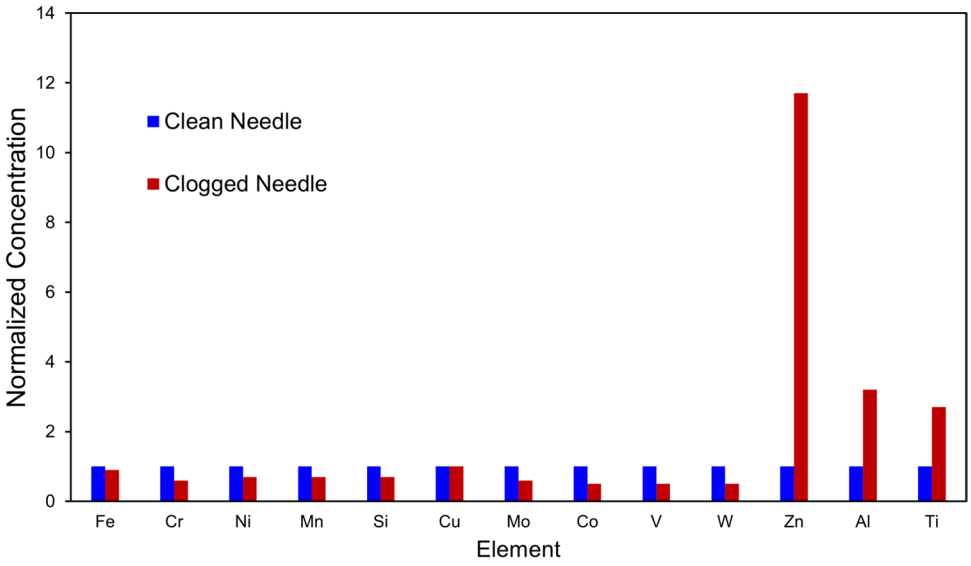


**Fig. 2** Metal contents in clean and clogged syringe conditioned at 40°C/75% RH for 3 months obtained by ICP-MS.

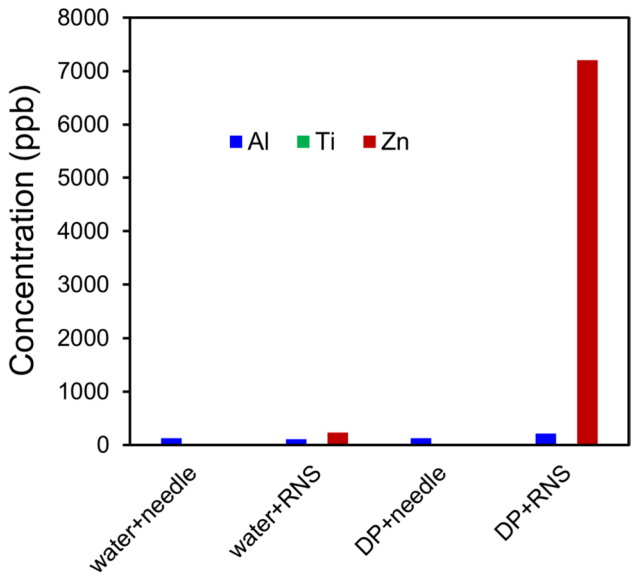


**Fig. 3** Migration of Al, Ti, and Zn for various combinations of sample stressed at 50°C for 10 days: (1) water and needle, (2) water and RNS, (3) drug product and needle, and (4) DP and RNS analyzed by ICP-MS.

we focus on Zn due to its precedence in inducing needle-clogging, however other elements may warrant study in a separate work. Each set consisted of varying combinations of water, DP, needles, and RNS, which were subsequently stored at a temperature of 50°C for a duration of 10 days. The set containing only water samples was utilized as the reference for comparative purposes. Based on the metal scan results from Fig. 2, Zn, Al, and Ti were tested in the samples and summarized in Fig. 3. Further evidence from Fig. 3 shows the migration patterns of Zn, Al, and Ti under various stress conditions at 50°C for 10 days. The results indicate that the combination of the drug product and the RNS facilitates the extraction of Zn ions. This suggests that the drug product demonstrates a favorable effect in extracting Zn from the RNS material, potentially contributing to the clogging issue observed in the needles. It is worth noting that among the oxidation states of zinc, the Zn(II) ion is highly soluble in water.

Despite observing slight variations in the levels of Al and Ti between clean and clogged needles, the concentrations of both metals were found to be extremely low and deemed negligible (~ 100 ppb Al and < 10 ppb Ti across all samples). Upon comparing the results of samples consisting of water and needles with those of water and RNS, it becomes apparent that the Zn originates from the RNS material. However, it should be noted that the leaching of Zn is limited in these circumstances. In contrast, when DP is introduced, there is a substantial increase in the concentration of Zn. This outcome provides evidence of an interaction between DP and RNS. When DP is present in the needle, and by extension likely in contact with the RNS, it seems to facilitate the extraction of Zn from the RNS material.

The RNS of PFSs is made of a rubber material, in which Zn oxide is generally used as the vulcanizing [23]. To further confirm that Zn leaches from the RNS, an SR-XRF analysis of a rubber used in RNS was performed. The sample was subjected to a high-intensity X-ray beam generated by a synchrotron. By analyzing the emitted fluorescent X-rays, the elemental composition of the sample can be determined. Indeed, the presence of Zn in rubber was confirmed as shown in Fig. 4. Other elements such as titanium (Ti), iron (Fe), rubidium (Rb), strontium (Sr) and zirconium (Zr) were also found. Zn and other heavy metal presence also align with the material datasheet provided by the RNS supplier. On the other hand, aluminum was not observed in RNS as the emitted fluorescent X-ray is below our detection limit.

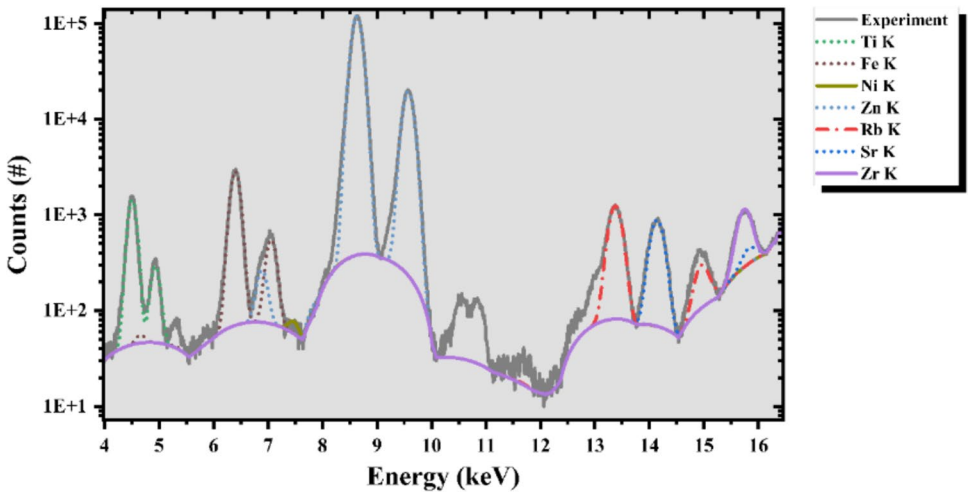


**Fig. 4** SR-XRF of a rubber material used in RNS. Measurement carried using X-ray energy 18.1 keV.

The results indicate a correlation between needle clogging and the elevated presence of Zn ions. Figures 2 and 3 demonstrate significant Zn migration into the drug product under various conditions, with the combination of the drug product and the RNS facilitating this extraction. Complementing these findings, Fig. 4's SR-XRF analysis reveals that the rubber material used in the RNS contains Zn. This association aligns with previous studies that also identify Zn content as a critical factor in needle clogging issues [13].

## High-resolution Imaging Analysis of the Needle Tip Containing Dried Drug Product

Visualizing the distribution of Zn is essential for identifying a possible source of needle clogging and providing insight into the concentration of Zn throughout the needle tip. 2D mapping using SR-XRF revealed that Zn accumulates in hotspots, indicated by arrows in Fig. 5. Corresponding SR-XPCT images of the same sample suggest that the Zn hotspots are composed of dried drug particles smaller than

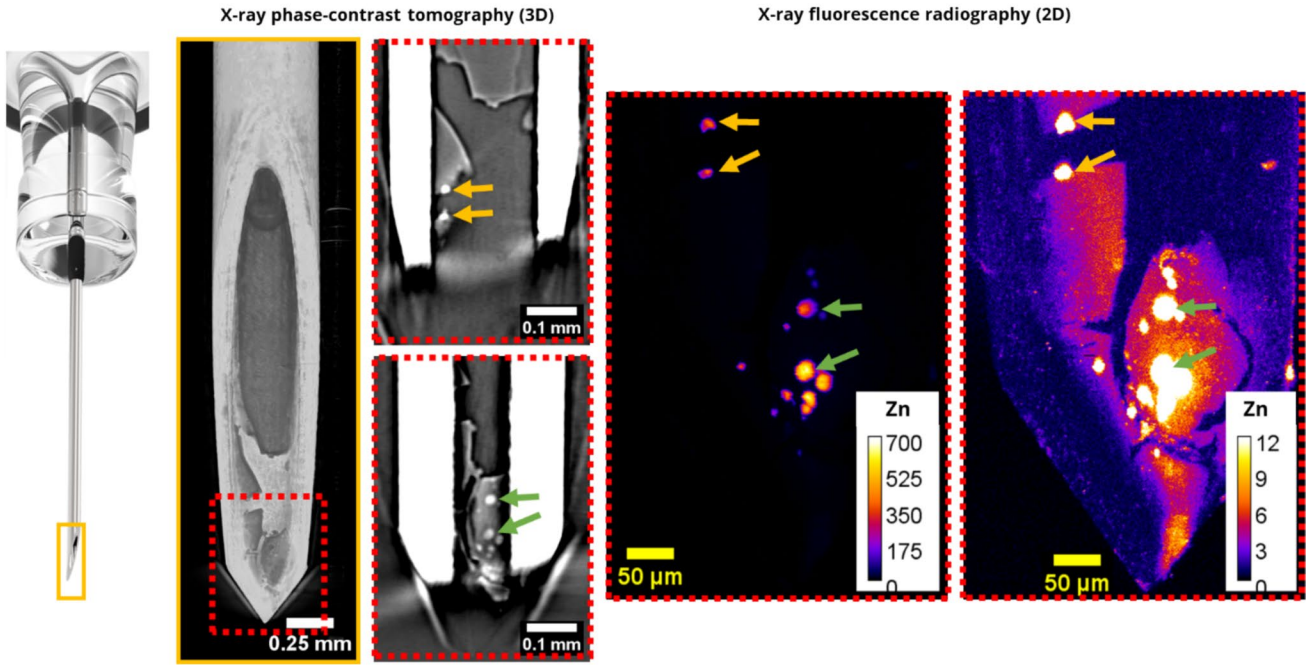


**Fig. 5** SR-XPCT and SR-XRF of a section of the needle tip containing dried drug staged for 4 months at 40°C. The SR-XPCT shows 3D distribution of the dried drug in the needle tip. Particles, which strongly attenuate X-ray were identified as Zn by using SR-XRF. SR-XPCT was performed with pixel size 2.75 µm and 35 keV X-ray beam. SR-XRF was done with pixel size 1 µm and 18.1 keV X-ray energy. The color bar shows the detector count for Zn.

20 µm. SR-XRF also shows Zn signal all over the dried drug, although the detector counts are substantially lower than for Zn particles. A comparison of SR-XRF and SR-XPCT confirms that Zn stays in the drug and does not enter the cracks in the dried formulation. Hence, Zn appears to migrate into the liquid drug accumulated in the needle tip during conditioning at 40°C. Further analysis of SR-XRF showed no other element in the dried drug, such as Ti, Fe, Cr, Rb, and Sr which were observed in the rubber of RNS (Fig. 4). Note that an X-ray beam energy of 18 keV was used and thus elements with higher ionization energies cannot be detected. In addition, aluminum found by ICP-MS (Fig. 2), cannot be measured by SR-XRF as the low-energy fluorescent X-rays are likely absorbed by the air before reaching the detector.

A whole needle tip of a syringe that was conditioned at 40°C for 4 months was scanned by SR-XRF, as shown in Fig. 6. As Zn was the only element observed in the dried drug, the energy of the X-ray was lowered from 18.1 to 12 keV increasing the sensitivity to Zn. In addition, the pixel size was increased from 1 to 4 µm to image the complete needle opening in a reasonable time, ca. 2 h. Optical microscopy and SR-XPCT images show that the dried drug was distributed in two separate volumes, one at the needle tip and a second one at the entrance to the needle, with an empty space in between. The Zn particles are observed in the needle tip. Note that SR-XRF does not capture the whole section of the dried drug at the entrance of the needle. This is because the secondary X-rays are hindered by the curved steel wall. The section with no signal (detector count is 0) of iron and nickel is shielded by the surrounding steel wall from which the secondary X-rays cannot escape as they are re-absorbed. Thus, the bottom section of the needle wall at the entrance to the needle appears black. Consequently, the dried drug can only be partially measured in this region as it sits on the wall. A thicker layer of the drug extends above the needle wall curvature, which allows the secondary X-rays to be collected by the XRF detectors. Although, this is a limitation of the used geometry, it nevertheless allows direct determination of the Zn distribution in as prepared needles without removing the dried drug.

Syringes conditioned at different time intervals: two, three, and four months were compared to reveal the impact of aging period on Zn migration (Fig. 6 and 7). In all clogged syringes that were imaged, Zn was found in the dried drug product. However, no trend was observed, likely due to re-absorption of the secondary X-rays by the steel wall. The signal strength for SR-XRF depended more on the position of the dried drug in reference to the needle tip. For example, the Zn count is higher when the drug peels away from the

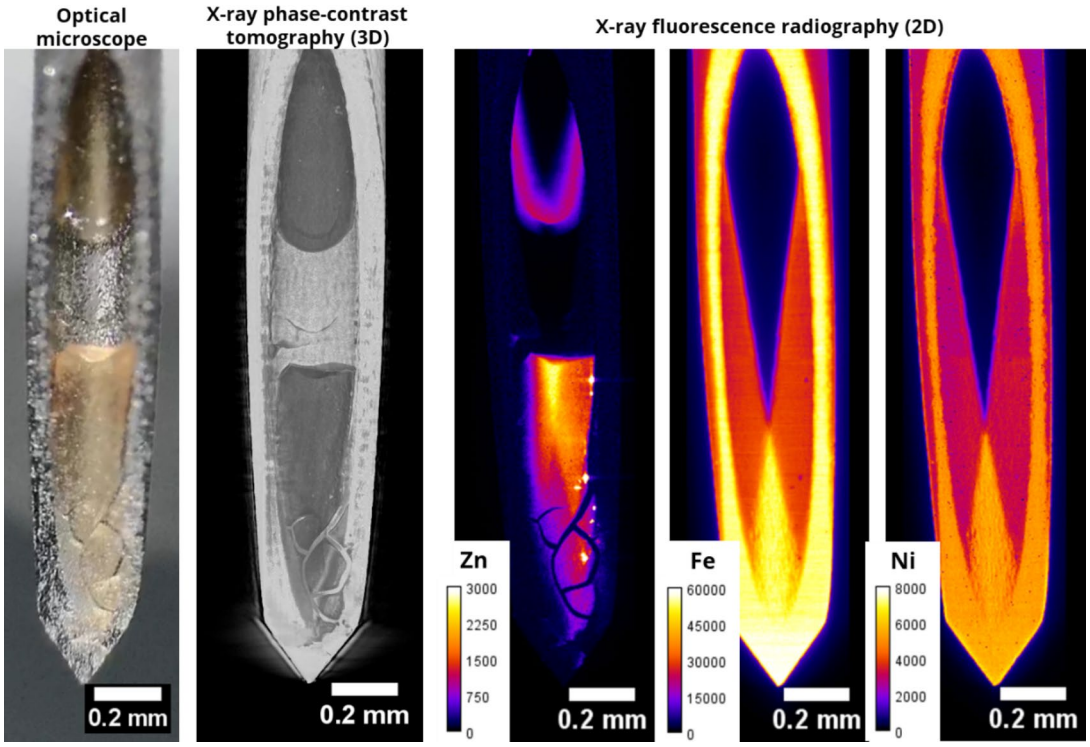


**Fig. 6** Dried drug in the needle tip imaged by optical microscope, SR-XPCT, and SR-XRF. The syringe was conditioned to 40°C for four months. Strongly attenuating Zn particles as well as Zn distributed in the dried drug are visible by SR-XRF. The maps of Fe and Ni show the shielding effect of the secondary X-rays by the curved steel needle wall. SR-XPCT was performed with pixel size 1.6 µm and X-ray energy 30 keV. SR-XRF was done with pixel size 4 µm and X-ray energy 12 keV. The color bar shows the detector count for the particular element.

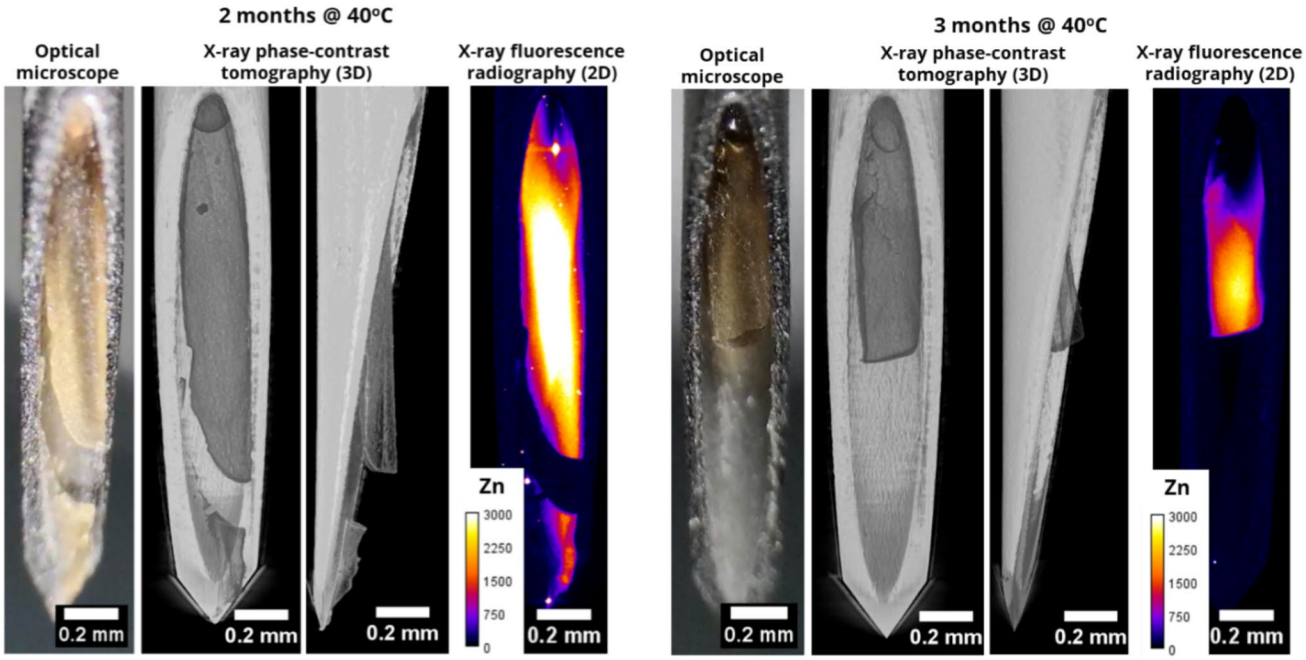


**Fig. 7** Dried drug in the needle tip of syringes exposed to 40°C for two (left column) and three (right column) months, respectively, Imaged by optical microscope, SR-XPCT, and SR-XRF. Zn, which migrated during conditioning into the drug is visualized by SR-XRF. Due to the shielding effect of the curved steel wall, the Zn signal is stronger for the drug layer delaminated from the needle. SR-XPCT was performed with pixel size 1.6 µm and X-ray energy 30 keV. SR-XRF was done with pixel size 4 µm and X-ray energy 12 keV. The color bar shows the detector count for Zn.

**Fig. 8** Dried drug in the needle tip of a syringe conditioned to 5°C for six months. The needle tip was imaged by optical microscope, SR-XPCT, and SR-XRF. Compared to conditioning at 40°C, Zn migration into the drug is very limited or none during the low temperature ageing. Low signal for Zn was observed around the steel wall, but no Zn was detected in the dried drug. SR-XPCT was performed with pixel size 1.6 µm and X-ray energy 30 keV. SR-XRF was done with pixel size 4 µm and X-ray energy 12 keV. The color bar shows the detector count for Zn.

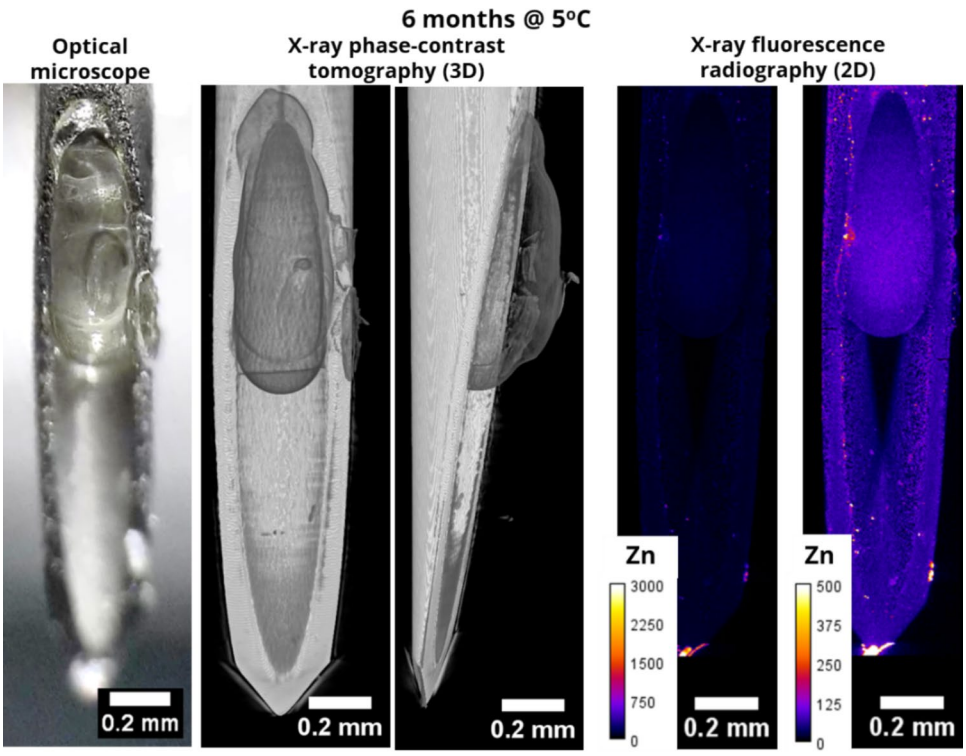

wall as it shrinks during drying, as observed in the syringe conditioned for 2 months in Fig. 7.

A syringe conditioned for six months at 5°C was investigated to determine the impact of temperature on Zn migration into the drug formulation, as shown in Fig. 8. Although the dried drug is located at the needle entrance, it extends above the curvature of the steel wall, which allows for the SR-XRF measurement. A low count of Zn was observed around the steel wall, but no Zn signal was visible in the dried drug itself. This suggests that at 5°C, the Zn migration rate is reduced such that on the timescale of 6 months, no detectable Zn was present in the dried drug. Interestingly, the clog in the needle tip is colorless on an optical microscopy image (Fig. 8), which differs from yellowish color of the clogs conditioned at 40°C (Fig. 6 and 7).

Correlation of 2D images from SR-XRF and 3D images from SR-XPCT reveals the location of Zn particles in the dried drug, Fig. 9. The particles are visible by SR-XPCT due to their higher X-ray attenuation than surrounding drug. The located Zn particles in 3D appear to be on the interface of the dried drug and air. These surfaces can be in close contact with RNS prior drying for an extended period of time, which indicates that Zn particles originate from the elastomer. During liquid evaporation, the drug product volume shrinks resulting in movement of the dried drug from the RNS.

## Discussion

Syringe clogging is a known issue observed in shelf-life studies and post-marketing events [7]. However, Zn has not been identified or quantified in clogged materials from real-life PFSs, and its precise location and distribution within needles remain unexplored. To address this gap and gain valuable information for further investigating the clogging

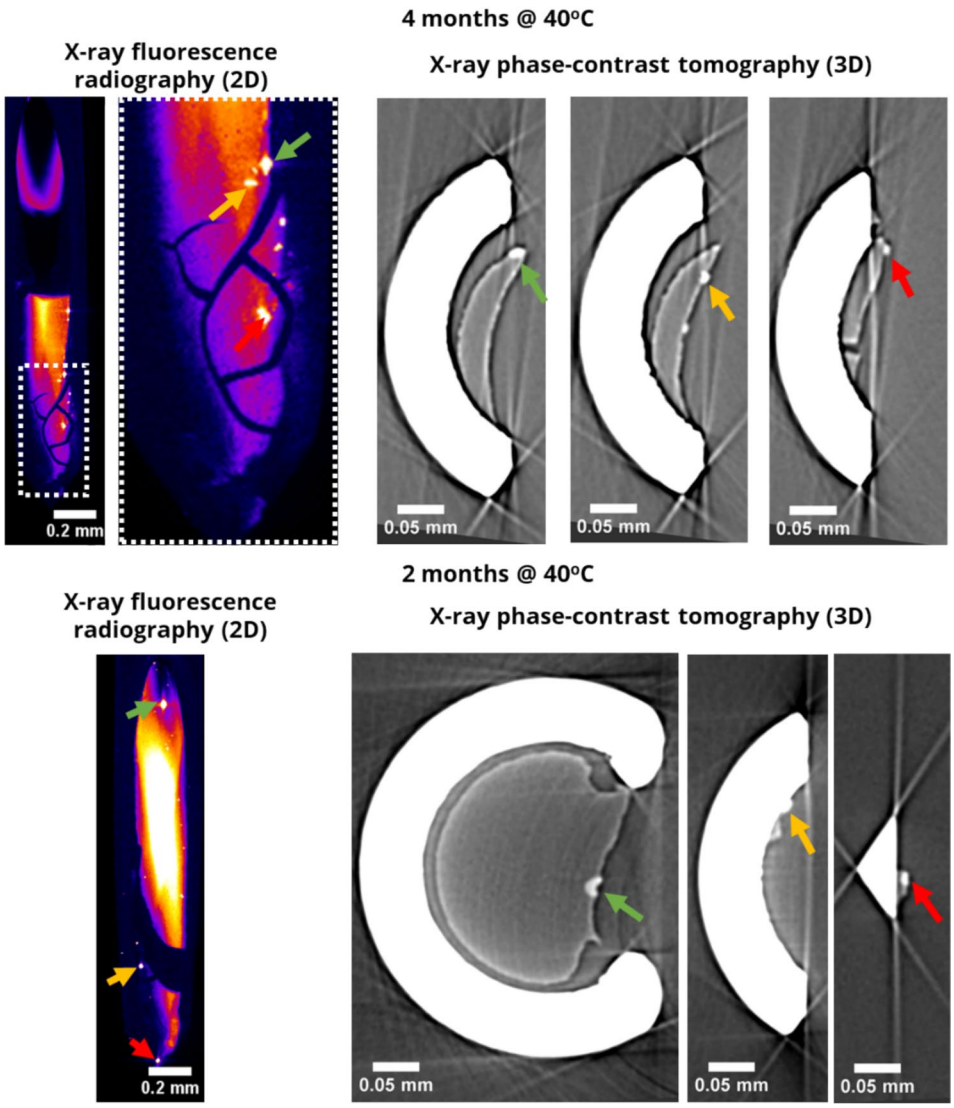


**Fig. 9** Zn particles identified in the needle tip by correlating 2D images from SR-XRF and 3D images from SR-XPCT for syringes exposed to 40°C for four months (top) and two months (bottom). The images show that the Zn particles are located on the interface of the dried drug and air. SR-XPCT was performed with pixel size 1.6 µm and X-ray energy 30 keV. SR-XRF was done with pixel size 4 µm and X-ray energy 12 keV.

mechanism, we utilized a series of advanced spectroscopy and imaging techniques capable of detecting or quantifying metal species in clogged materials *ex situ* or *in situ* in PFSs. The results obtained from these techniques provide a comprehensive mapping of Zn migration from the elastomer in the RNS into the drug products. Specifically, the chemical resolution of SR-XRF enabled the identification of metal species in the elastomer, with a notable presence of Zn (Fig. 4). ICP-MS further quantified Zn as the most abundant metal found in the clogged material from the needle (Fig. 2). When comparing water and drug product soaking in the RNS, the drug product appeared to extract Zn more efficiently (Fig. 3).

Additionally, we determine that Zn migration from the RNS to the drug product and the resulting inhomogeneities due to interactions with the needle tip is a kinetic process, dependent on drying rate given leaching is limited in solid materials [13]. Furthermore, we demonstrate in our previous work that the drug product morphology and presence in the needle tip are highly variable, and air gaps and bubble formation can be present [10]. These air gaps result in the lack of long-term or smooth migration of Zn into the drug product.

To analyze the presence and distribution of Zn in the needle of pre-filled syringes, we employed SR-XPCT with pixel size of 1.6 µm or 2.75 µm and SR-XRF with pixel sizes of 1 or 4 µm. We observed Zn in the clogged material of needles containing drug product stressed at 40°C (Figs. 5 and 6). Zn migration seemed to occur as early as two months under these elevated stress conditions (Fig. 7). Further imaging analysis identified Zn particles at the interface between the drug and RNS (Fig. 9), suggesting the particles originate from the elastomer. Interestingly, samples stored at 5°C did not show Zn presence in the dried drug product (Fig. 8), suggesting temperature plays a role in Zn release and migration. In addition, the optical microscope images showed the clog is colorless in the samples stored at 5°C compared to yellowish dried drug in syringes stressed at 40°C, which suggests the different impact on the drug product with and without the Zn presence.

These findings pinpoint the polymer material of the RNS as the source of Zn ions and allow visualization of the migration of Zn into the drug product, based on both ex-situ and in-situ analysis of the clogged materials. This discovery provides insight into the mechanism behind the clogging by viscosity increase [13], tracing the Zn migration pathway from the device component into the drug product. It further highlights the necessity of eliminating contact between the mAb solution and the elastomer at the needle tip to prevent potential clogging risks. Additionally, one critical observation is the temperature dependence of Zn extraction observed at 40°C, a typical stress condition, emphasizing the importance of lower storage temperatures in ensuring product stability and quality. Moreover, the drug product was found to extract Zn more efficiently than water, suggesting a mechanistic role for the mAb or formulation excipients. Our follow-up studies will focus on identifying the critical components that facilitate Zn ion extraction to better understand the mechanism of needle-clogging.

Moreover, the data revealed Zn hotspots within the dried drug, as indicated by SR-XRF imaging. These hotspots, likely Zn particles smaller than 20 µm, were observed to remain within the drug matrix and did not enter cracks in the formulation. This observation suggests that Zn migrates into the liquid phase of the drug concentrated at the needle tip, potentially contributing to clogging issues. However, to accurately quantify these Zn deposits and their impact, ICP-MS analysis is imperative. According to elastomer specifications, the target Zn concentration is < 5.0 µg/mL DP in solution [23]. Our ICP-MS analysis reveals a Zn content of 0.350 µg in the 0.24 mg of material clogging the needle. Given the total filling volume of the needle, which can be calculated based on its dimensions, a diameter of 275 µm and a length of 12.7 mm, the volume amounts to approximately 0.000754 ml. Consequently, the calculated zinc concentration in the clogged material is approximately 464 µg/ml (0.350 µg/0.000754 ml). This concentration is significantly higher than the targeted specifications, exceeding them by nearly 100 times. However, it is unlikely that liquid formulation fills the entire volume of the needle uniformly. Therefore, the local concentration of the formulation within the needle could be even higher than this calculated value. SR-XRF imaging also reveals the hotspots and heterogeneity of the sample indicate regions of much greater Zn content than desired, which may lead to regions of greater Zn-induced gelation.

Finally, our study effectively leveraged the capabilities of advanced analytical techniques in a complementary manner, providing valuable insights and experiences for investigating clogging issues. We summarize these techniques and each of their advantages in Table II. The imaging techniques, including SR-XRF and SR-XPCT, allowed for *in situ* imaging of clogging materials within the needle. Specifically, SR-XPCT provided high-resolution information regarding the location of clogged materials and detailed morphological insights. SR-XRF, with its fluorescence detection capability, identified the distribution of metals within the clogged materials inside the needle.

While imaging techniques offer high-resolution, elemental mapping, they lack the ability to precisely quantify Zn content by weight or ion count within the entire clogged needle sample. For instance, a limitation of SR-XRF is its inability to measure the total amount of Zn, particularly when unknown quantities may adhere to the interior of the needle or remain undetected within the removed dried formulation due to secondary X-ray reabsorption caused

**Table II** Techniques that Analyze Needle Tips and Clogged Material

| Techniques | Non-invasive analysis | Measurements | Quantitative | Pixel size | Chemical resolution |
|---|---|---|---|---|---|
| ICP-MS | No | Metal elemental content | Yes | N/A | Yes |
| Optical microscopy | Yes | Visualization of clogged material | No | 3 µm | No |
| Synchrotron-based X-ray Fluorescence | Yes | Elemental Mapping | Very challenging in the used geometry | 1 µm | Yes |
| Synchrotron-based X-ray Phase-Contrast Computed Tomography | Yes | High-resolution tomographic imaging in 3D | No | 1.6 µm | No |
| Neutron Imaging | Yes | Needle penetration view of liquid | No | 13.5 µm | No |

by the needle tip geometry. Furthermore, SR-XRF signal intensity is significantly influenced by the positional height of the dried drug product, as secondary X-rays require an unobstructed path to the detector. An alternative approach could be the use of scanning SR-XRF tomography, which would allow to retrieve the elemental distribution in 3D. However, that would be significantly limited to the sample surface in the present system, due to the strong absorption of the steel. These factors complicate the assessment of Zn content, as SR-XRF primarily captures surface elements and cannot detect deeper or interior Zn deposits within the needle or drug matrix. Quantitative XRF reading would require accounting for the matrix effect of the materials, calibration, reference standards, and a way to circumvent the enclosed geometry of the sample [24].

In contrast, ICP-MS emerged as the quantitative method capable of accurately measuring Zn ions in the samples analyzed in this study. With its high sensitivity and precision, ICP-MS is indispensable for quantifying Zn content in both the drug formulation and any accumulated deposits within the needle by removing the needle clog. By combining SR-XPCT for spatial distribution, SR-XRF for chemical mapping with ICP-MS for precise quantification, we developed a robust framework for investigating Zn behavior. This complementary approach provides understanding of Zn migration from the RNS, addressing both qualitative and quantitative aspects of the phenomenon.

## Conclusion

Our study provides insights into the mechanisms underlying Zn migration and its potential role of needle clogging in staked-in-needle PFSs. Utilizing advanced analytical techniques such as SR-XPCT, SR-XRF, and ICP-MS, we confirm that Zn leaches from the RNS and accumulates in the dried drug formulations, particularly under elevated temperature conditions. While Zn is not proposed as the sole factor causing needle clogging, its origin in the RNS and unexpected presence in the dried drug product underscore its potential role in contributing to this issue. Further research is required to comprehensively understand the multifactorial nature of needle clogging in PFSs, particularly the potentially distinct impact of individual formulation components in extracting Zn from the RNS. These findings enhance our understanding of the chemical factors contributing to needle clogging and provide a foundation for developing effective mitigation strategies, ultimately improving the performance and reliability of PFSs.

**Funding** This work is supported by Merck Sharp & Dohme LLC, a subsidiary of Merck & Co., Inc., Rahway, NJ, USA.

## Declarations

**Competing Interests** The authors declare there is no conflict of interest.



## References

1. Wang SS, Yan Y, Ho K. US FDA-approved therapeutic antibodies with high-concentration formulation: summaries and perspectives. Antib Ther. 2021;4(4):262–73.
2. Garidel P, Kuhn AB, Schäfer LV, Karow-Zwick AR, Blech M. High-concentration protein formulations: How high is high? Eur

J Pharm Biopharm. 2017;119:353–60. https://doi.org/10.1016/j.ejpb.2017.06.029.
3. Allmendinger A, Fischer S, Huwyler J, Mahler HC, Schwarb E, Zarraga IE, *et al*. Rheological characterization and injection forces of concentrated protein formulations: An alternative predictive model for non-Newtonian solutions. Eur J Pharm Biopharm. 2014;87(2):318–28.
4. Kowsari K, Lu L, Persak SC, Hu G, Forrest W, Berger R, *et al*. Injectability of high concentrated suspensions using model microparticles. J Pharm Sci. 2024;113(12):3525–37.
5. Adamis Pharmaceuticals Corporation Issues Nationwide Voluntary Recall of SYMJEPI® (Epinephrine) Injection for Potential Manufacturing Defect | FDA [Internet]. Available from: https://www.fda.gov/safety/recalls-market-withdrawals-safety-alerts/adamis-pharmaceuticals-corporation-issues-nationwide-voluntary-recall-symjepir-epinephrine-injection. Accessed 31 Jul 2024.
6. Sánchez-Félix M, Burke M, Chen HH, Patterson C, Mittal S. Predicting bioavailability of monoclonal antibodies after subcutaneous administration: Open innovation challenge. Adv Drug Deliv Rev. 2020;167:66–77.
7. Therapeutic Biological Establishment Evaluation Request (TBEER) Form. 2013;0–29. Available from: https://www.accessdata.fda.gov/drugsatfda_docs/nda/2012/125276Orig1s049ChemR.pdf. Accessed 30 Dec 2024.
8. De Bardi M, Müller R, Grünzweig C, Mannes D, Boillat P, Rigollet M, *et al*. On the needle clogging of staked-in-needle pre-filled syringes: Mechanism of liquid entering the needle and solidification process. Eur J Pharm Biopharm. 2018;128(May):272–81.
9. De Bardi M, Müller R, Grünzweig C, Mannes D, Rigollet M, Bamberg F, *et al*. Clogging in staked-in needle pre- filled syringes (SIN-PFS): Influence of water vapor transmission through the needle shield. Eur J Pharm Biopharm. 2017;2018(127):104–11.
10. Hu G, Bonanno D, Su Y, Zhao X, Krishnamachari Y, Forrest W, et al. Unraveling Pre-filled Syringe Needle Clogging : Exploring a Fresh Outlook Through Innovative Techniques. Pharm Res [Internet]. 2024;(March 2022). https://doi.org/10.1007/s11095-024-03673-7
11. Scheler S, Knappke S, Schulz M, Zuern A. Needle clogging of protein solutions in prefilled syringes: A two-stage process with various determinants. Eur J Pharm Biopharm. 2022;1(176):188–98.
12. De Bardi M, Müller R, Grünzweig C, Mannes D, Rigollet M, Bamberg F, *et al*. Clogging in staked-in needle pre- filled syringes (SIN-PFS): Influence of water vapor transmission through the needle shield. Eur J Pharm Biopharm. 2017;2018(127):104–11.
13. Fukuda M, Yamazaki T, Ueno S, Koga A, Yamanaka Y. Viscosity increase / gelation of therapeutic IgG monoclonal antibodies induced by Zn 2+: One possible root cause of clogging of staked-in-needle prefilled syringes. Eur J Pharm Biopharm. 2022;178(August):179–86.
14. Kaestner A, Roth J, Grünzweig C. Real-Time Neutron Imaging to Detect Origin of Blocking in Drug Injection Devices. PDA J Pharm Sci Technol. 2016;70(4):353–60.
15. Cloetens P, Barrett R, Baruchel J, Guigay JP, Schlenker M. Phase objects in synchrotron radiation hard x-ray imaging. J Phys D Appl Phys [Internet]. 1996;29(1):133. Available from: https://iopscience.iop.org/article/10.1088/0022-3727/29/1/023. Accessed 31 Jul 2024.
16. Bonaventura F, Scheler S, Novak V, Olbinado MP, Wagner M, Grünzweig C, *et al*. Does needle clogging change the spatial distribution of injected drug in tissue? New insights by X-ray computed tomography. Eur J Pharm Biopharm [Internet]. 2025;207. Available from: https://pubmed.ncbi.nlm.nih.gov/39694077/. Accessed 10 Mar 2025.
17. Patterson C, Murphy D, Irvine S, Connor L, Rattray Z. Novel application of synchrotron x-ray computed tomography for ex-vivo imaging of subcutaneously injected polymeric microsphere suspension formulations. Pharm Res [Internet]. 2020;37(6):1–11. Available from: https://link.springer.com/article/10.1007/s11095-020-02825-9. Accessed 10 Mar 2025.
18. Fukuda M, Yamazaki T, Ueno S, Koga A, Yamanaka Y. Viscosity increase / gelation of therapeutic IgG monoclonal antibodies induced by Zn 2+: One possible root cause of clogging of staked-in-needle prefilled syringes. Eur J Pharm Biopharm. 2022;178(August):179–86. https://doi.org/10.1016/j.ejpb.2022.08.008.
19. Clases D, Gonzalez de Vega R. Facets of ICP-MS and their potential in the medical sciences—Part 2: nanomedicine, immunochemistry, mass cytometry, and bioassays. Anal Bioanal Chem. 2022;414(25):7363–86. https://doi.org/10.1007/s00216-022-04260-8.
20. Rodrigues C, Alves C, Santos-neto AJ, Fernandes C, Lan FM. Inductively coupled plasma mass spectrometry (ICP MS): a versatile tool. J Mass Spectrom. 2007;42(4):419–27.
21. Gentile K, Huang C, Liu X, Whitty-Léveillé L, Hamzaoui H, Cristofolli E, *et al*. Variables Impacting Silicone Oil Migration and Biologics in Prefilled Syringes. J Pharm Sci. 2023;112(8):2203–11.
22. European Pharmacopoeia Commission. 3.2. 9 rubber closures for containers for aqueous parenteral preparations, for powders and for freeze dried powders. Eur Pharmacopoeia. 2005;9:5545–6.
23. Chandrasekaran VC. Rubbers, chemicals and compounding for 'O' rings and seals. In: Rubber seals for fluid and hydraulic systems. 2010. p. 57–69. https://doi.org/10.1016/B978-0-8155-2075-7.10006-1.
24. Vanhoof C, Bacon JR, Ellis AT, Vincze L, Wobrauschek P. 2023 atomic spectrometry update-a review of advances in X-ray fluorescence spectrometry and its special applications. J Anal At Spectrom. 2023;38:1730–43.